

Supplementary Material  
for

## **Scaffolded Amino Acids as a Close Structural Mimic of Type-3 Copper Binding Sites**

H. Bauke Albada, Fouad Soulimani, Bert M. Weckhuysen, Rob M.J. Liskamp\*

H.B. Albada and prof. dr. R.M.J. Liskamp, Medicinal Chemistry and Chemical Biology,  
Utrecht Institute of Pharmaceutical Sciences, Faculty of Science, Utrecht University,  
Sorbonnelaan 16, 3584 CA Utrecht, The Netherlands.

F. Soulimani and prof. dr. ir. B.M. Weckhuysen, Inorganic Chemistry and Catalysis group,  
Faculty of Science, Utrecht University, Sorbonnelaan 16, 3584 CA Utrecht, The Netherlands.

\* to whom correspondence should be addressed: [r.m.j.liskamp@uu.nl](mailto:r.m.j.liskamp@uu.nl)

### **General Information**

Chemicals were obtained from commercial sources and used without further purification. Reactions were performed at room temperature. Solution phase reactions were monitored by TLC analysis and  $R_f$ -values were determined on Merck pre-coated silica gel 60 F-254 (0.25 mm) plates. Spots were visualized with UV-light. Solid-phase synthesis was carried out in plastic syringes with PE frit (20  $\mu\text{m}$ ), Applied Separations Inc., distributed by Alltech Applied Science Group (Hoogeveen, The Netherlands). Column chromatography was carried out using Silica-P Flash silica gel (60  $\text{\AA}$ ; particle size 40-63  $\mu\text{m}$ ; Silicycle). Electrospray Ionisation mass spectrometry (ESI-MS) was performed on a Finnigan LCQ Deca XP MAX LC/MS system. HPLC was performed on a Shimadzu Class-VP automated high performance liquid system, using an analytical reverse-phase column (Alltima, C8, 300  $\text{\AA}$ , 5  $\mu\text{m}$ , 250  $\times$  4.6 mm) and a UV-detector (operating at 220 and 254 nm) and an ELSD-detector. Elution was realized using a gradient from water/MeCN/TFA – 95/5/0.1 % (v/v) to MeCN/water/TFA – 95/5/0.1 % (v/v) in 20 min and at a flow rate of 1 mL/min.

A pH-meter used was the PHM120 standard pH meter from Meterlab, standard analytical was used. Microtiterplate reader was from BioTek mQuant (Beun De Ronde, Abcoude, The Netherlands). The UV/vis microtiterplate was from Greiner bio-one (Alphen aan de Rijn, The Netherlands). Software used for data analysis was the Full Mode-KC4 (Version 3.4 (Rev 21)) software (BioTek instruments) and data point resolution was set at 2 nm. IR spectra were recorded on a Bruker Tensor 37 FT-IR spectrometer with a DTGS detector using KBr pellets, at a point resolution of 4  $\text{cm}^{-1}$ . Raman spectra were recorded on a Kaiser RXN spectrometer equipped with a 785 nm diode laser was used in combination with a Hololab 5000 Raman microscope. A 10 $\times$  objective was used for beam focusing and collection of scattered radiation. The laser output power was 70 mW. The data point resolution was about 2  $\text{cm}^{-1}$  and 10 scans were accumulated with an exposure time of 30 s for each spectrum. The setup for diffuse reflection measurements is based on an Olympus BX41 upright research microscope with a 50 $\times$ , 0.5 NA high working distance microscope objective. A 75 W Xenon lamp is used for illumination. The microscope was equipped with a 50/50 double viewport tube, which accommodates a CCD video camera (ColorViewIIIu, Soft Imaging System GmbH) and an optical fiber mount. A 200 micrometer-core fiber connects the microscope to a CCD UV/vis spectrometer (AvaSpec-2048TEC, Avantes BV). 10 scans were collected with an integration time of 50 ms per scan.

## Synthesis

### Synthesis of the ligand

The synthesis of the scaffold has been described in detail elsewhere<sup>1</sup>. For the synthesis of the tris(histidine-acetyl) ligand on the solid-phase, several standard procedures were applied. For each gram of resin roughly 6 mL of solvent/solution (stored on 4 Å molsieves) was used:

- Fmoc-removal: 20% piperidine/NMP was used (2 × 6 mL each 8 min), after which the resin was washed with NMP (3 × 6 mL each 2 min) and DCM (3 × 6 mL each 2 min). Fmoc removal was monitored using a Kaisertest<sup>2</sup>.

- Coupling of acids: 3 eq of scaffold or 4 eq Fmoc-His(Trt)-OH was used together with 3 or 4 eq BOP and 6 or 8 eq DiPEA, respectively, in NMP. Coupling was performed overnight in case of HO-TAC(*o*NBS)<sub>3</sub> and for 3 h in case of Fmoc-His(Trt)-OH and. The resin was washed with NMP (3 × 6 mL each 2 min) and DCM (3 × 6 mL each 2 min). Coupling was monitored using the Kaisertest in case of coupling to primary amines and the Chloranil<sup>3</sup> test in case of coupling to secondary amines.

- *o*NBS-removal<sup>4</sup>: prior to deprotection, the resin was washed with DMF (3 × 6 mL each 2 min). After this, a solution of 2-mercaptoethanol (0.5 M in DMF: 6 mL; 3 mmol) to which DBU (224 μL; 1.5 mmol) was added (3 × 30 min). Subsequently, the resin was washed with DMF (3 × 6 mL each 2 min) and DCM (3 × 6 mL each 2 min) and the liberated amines were detected using the Chloranil test.

- Acetylation: A freshly prepared solution was applied in order to acetylate the *N*-terminal amine. This solution consists of Ac<sub>2</sub>O (14.2 mL), DiPEA (6.5 mL) and HOBt (608 mg). After the acetylation the resin was washed with NMP (3 × 6 mL each 2 min) and DCM (3 × 6 mL each 2 min).

- Deprotection and cleavage: The ligand was deprotected on the histidine side-chains and simultaneously removed from the resin using 3 mL TFA/TIS/H<sub>2</sub>O – 92.5/5/2.5 (v/v).

For the synthesis 1 g of PS-S RAM-Fmoc resin (loading = 0.78 mmol/g) was used and the reactions were performed in a syringe with frit. Firstly, the Fmoc-group was removed and the scaffold was attached overnight. Remaining amines on the resin were capped by acetylation followed by removal of the *o*NBS-groups<sup>5</sup>. After this, Fmoc-His(Trt)-OH was coupled under identical conditions twice, in order to ensure complete reaction with the scaffold. The Fmoc-group was removed and the *N*-terminal amine was acetylated. The ligand was deprotected and removed from the resin, precipitated in MTBE/hexanes – 1/1 and purified by column chromatography (CHCl<sub>3</sub>/MeOH/25% NH<sub>4</sub>OH – 8/4/1.5 (v/v)). The pure fractions were concentrated and lyophilized from water with pH 7. Purity of the ligand was assessed by TLC and HPLC and the identity confirmed by ESI-MS. *R*<sub>f</sub> = 0.67 (CHCl<sub>3</sub>/MeOH/25% NH<sub>4</sub>OH - 60/45/20 (v/v)). ESI-MS: *m/z* = 837.39 [2M+2Na]<sup>2+</sup> (calculated M+Na: 836.39 (EM) and 836.89 (FW)) and 815.13 [2M+2H]<sup>2+</sup> (calculated M+H: 814.40 (EM) and 814.91 (FW)).

<sup>1</sup> M.C.F. Monnee, A.J. Brouwer and R.M.J. Liskamp, *QSAR & Combinatorial Sciences*, 2004, **23**, 546.

<sup>2</sup> E. Kaiser, R.L. Colescott, C.D. Bossinger, P.I. Cook, *Anal. Biochem.*, 1970, **34**, 595; V.K. Sarin, S.B.H. Kent, J.P. Tam, R.B. Merrifield, *Anal. Biochem.*, 1981, **117**, 147.

<sup>3</sup> T. Vojtkovsky, *Pept. Res.*, 1995, **8**, 236.

<sup>4</sup> S.C. Miller, T.S. Scanlan, *J. Am. Chem. Soc.*, 1997, **119**, 2301; J.F. Reichwein, R.M.J. Liskamp, *Tetrahedron Lett.*, 1998, **39**, 1243.

<sup>5</sup> See also T. Fukuyama, C.-H. Tow, M. Cheung, *Tetrahedron Lett.*, 1998, **39**, 1243.

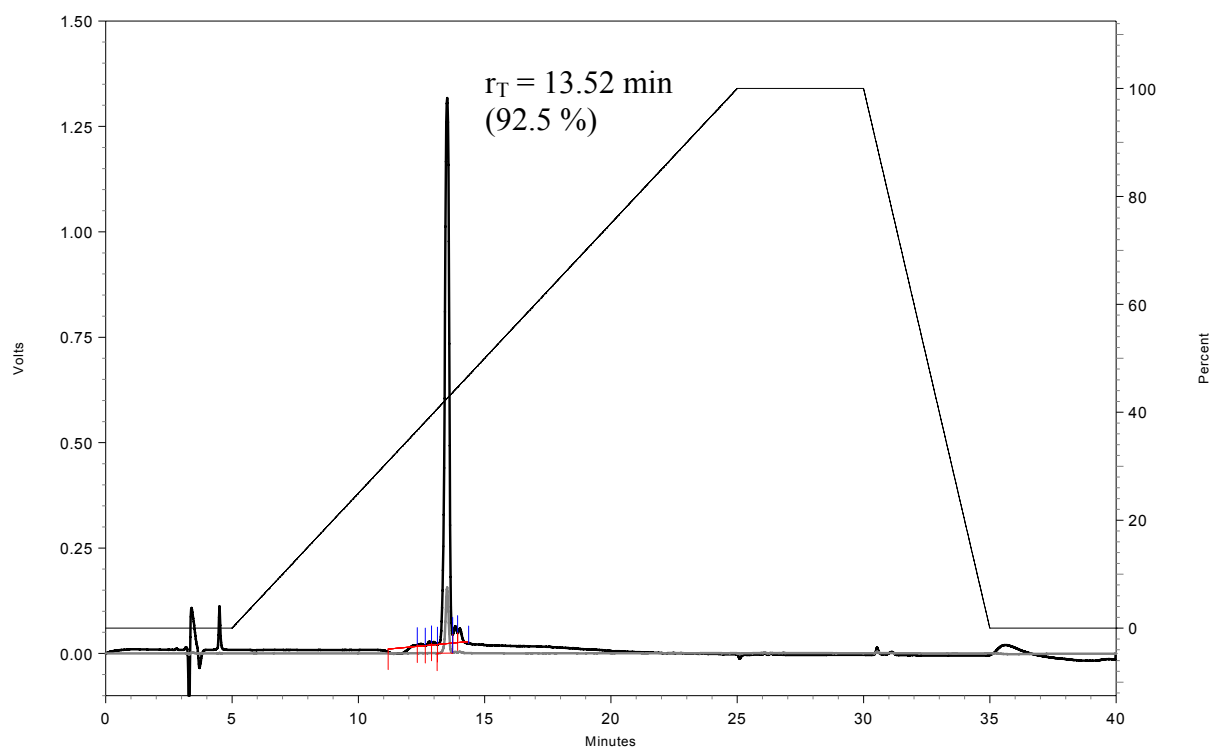


**Figure S1** – HPLC trace of the ligand. Detection with UV: 254 nm (upper trace; black) and 220 nm (lower trace; grey).

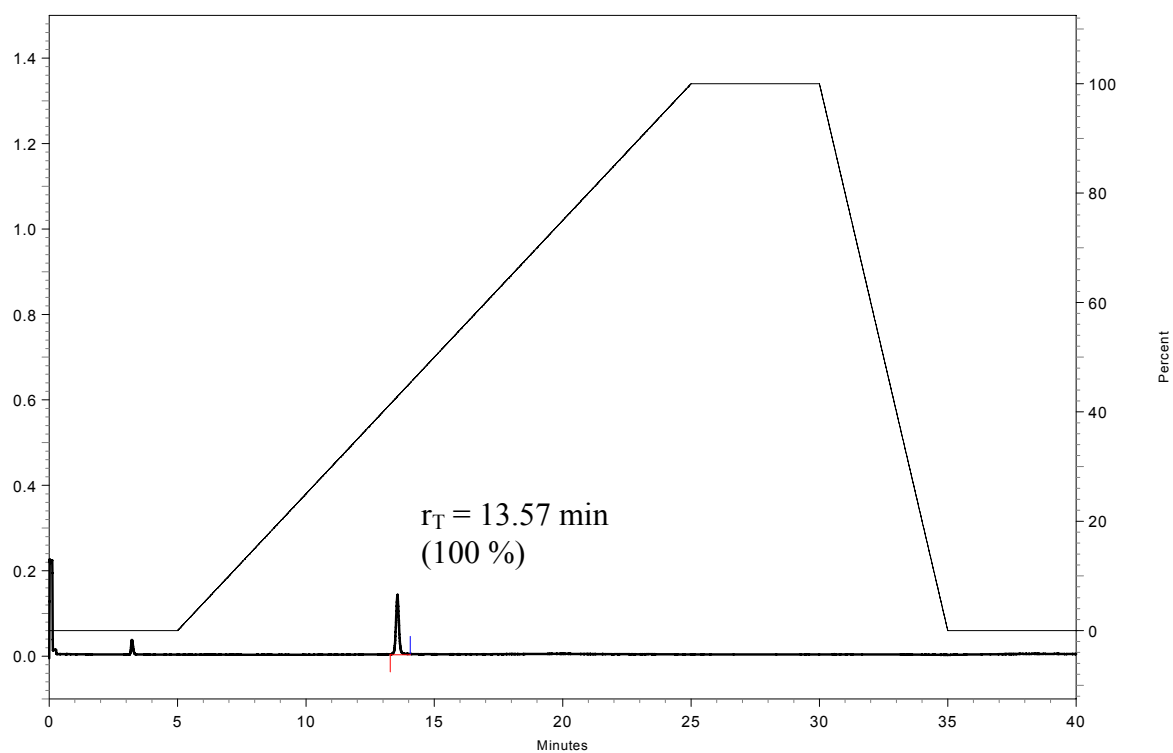


**Figure S2** – HPLC-traces of the ligand (detection with ELSD).

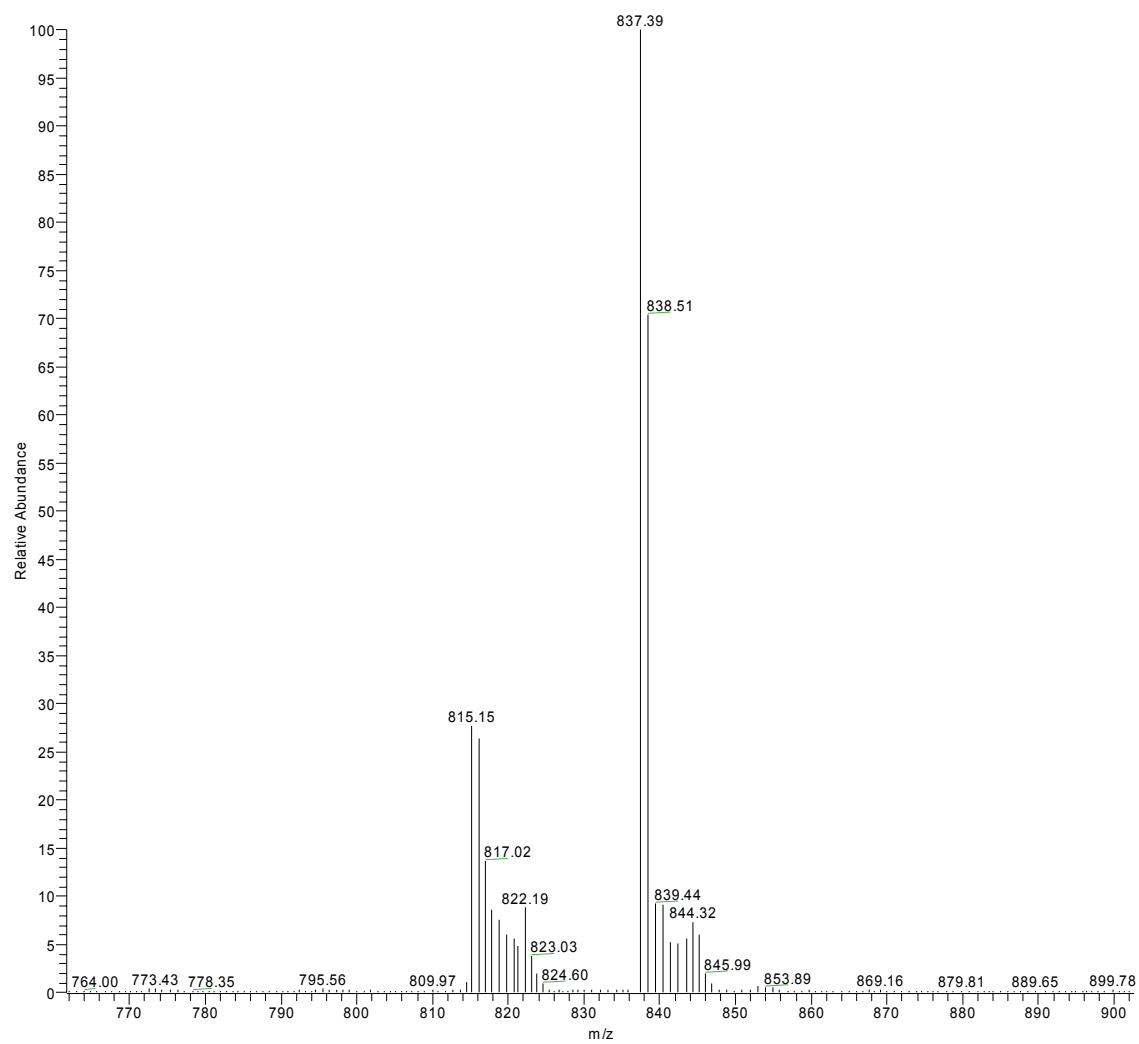


**Figure S3** – ESI-MS spectrum of the ligand:  $815.15 = [2M+2H]^{2+}$  and  $837.39 = [2M+2Na]^{2+}$ .

## pH-titrations

In order to gain insight in the  $pK_a$ -values of the individual imidazole rings of the tridentate ligand, a pH-titration on both ligand and complex was performed. To a 25 mM solution of the ligand, 5  $\mu$ L of 0.5, 1, 2, 3, 4 or 5% of  $\text{NaHCO}_3$  was added and the pH was measured. The concentration of the added base was adjusted depending on the observed shift in pH.

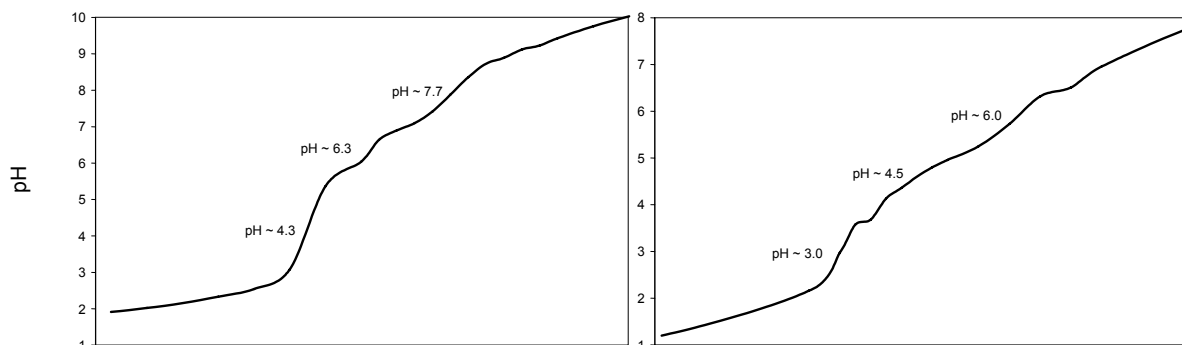


**Figure S4** – pH-titration curves of the ligand (left) and the complex (right). The three different protonation states of both ligand and complex can be clearly seen.

### Ligand:

- $\text{pH} > 4.3$ :  $[\text{ligH}_3]^{3+}$ ;
- $4.3 < \text{pH} < 6.3$ :  $[\text{ligH}_2]^{2+}$ ;
- $6.3 < \text{pH} < 7.7$ :  $[\text{ligH}]^+$ ;
- $\text{pH} > 7.7$ :  $[\text{lig}]$ .

The first imidazole ring of the ligand starts to become deprotonated at  $\text{pH} \sim 3$ , with  $pK_a \sim 4.3$ , which is roughly two units below the  $pK_a$  of isolated histidine side-chains. Apparently, the close proximity of the histidinyl imidazole rings causes a strong electrostatic repulsion between the charges, resulting in this low  $pK_a$ . The second proton is released at a  $pK_a$  close to the  $pK_a$  of isolated histidine (6.3 vs. 6.5). At roughly 1 unit above the  $pK_a$  of histidinyl imidazole rings (7.7), the last proton is liberated.

### Complex:

Significant differences in  $pK_a$  are found when one equivalent of  $\text{Cu(II)}$  is added:

- $\text{pH} > 3.0$ :  $[\text{ligH}_3]^{3+}$ ;
- $3.0 < \text{pH} < 4.5$ :  $[\text{ligCuH}_2]^{4+}$ ;
- $4.5 < \text{pH} < 6.0$ :  $[\text{ligCuH}]^{3+}$ ;
- $\text{pH} > 6.0$ :  $[\text{ligCu}]^{2+}$ .

The presence of  $\text{Cu(II)}$  shifts the  $pK_a$ 's down about 1.7 units; the first  $pK_a$  is least affected since  $\text{Cu(II)}$  is not yet coordinating to the ligand. After the first imidazole ring of the ligand has been coordinated to copper(II), the other protonated imidazole rings are easily deprotonated, resulting in  $pK_a$ 's of 4.5 and 6.0. Coordination of the copper(II)-ion to one histidine side chain results in a total charge of the complex of 4+. Obviously, this is a very unfavorable situation which is resolved by lowering the  $pK_a$ 's of the other imidazole rings.

## Spectroscopic studies

### Determining coordinating atoms:

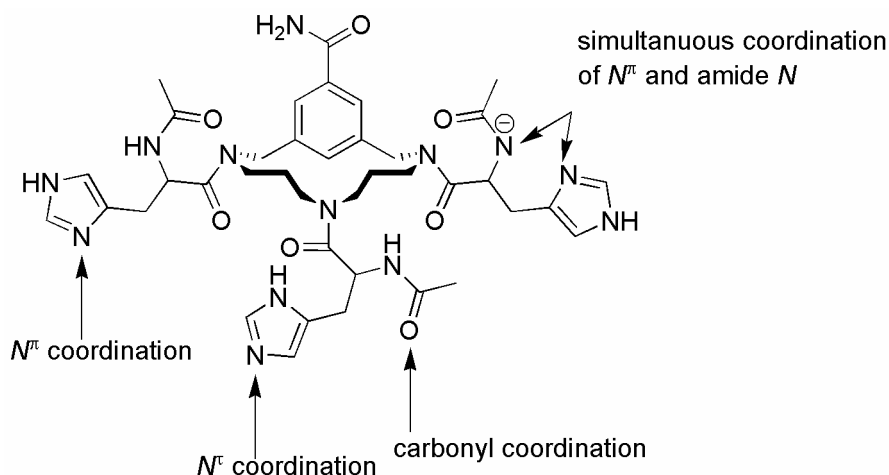


**Figure S5** – Coordination possibilities of the TAC-based hemocyanin mimic. UV/vis can distinguish between coordination with carbonyl oxygen, imidazole and amide nitrogen atoms. It cannot distinguish between the two imidazole nitrogen atoms.

### **UV/vis absorption spectrum**

Complexation studies were carried out by measuring 5 mM (for the charge-transfer absorption bands) and 25 mM (for the *d-d* transition bands) solutions of the 1:1 mixture of the ligand and the copper(II) salt. This was done by adding 50  $\mu$ L of each of the solutions of both ligand and Cu(SO<sub>4</sub>)·5H<sub>2</sub>O in water (10 mM or 50 mM) to the same well of the microtiterplate. The mixture was acidified by the addition of a dilute solution of HCl. In order to obtain spectra at different pH's, 5  $\mu$ L of a 5% solution of NaHCO<sub>3</sub> in water was added, the pH was measured and the spectrum obtained over a range of 200-998 nm. With increasing pH a distinct increase in intensity of the blue color was observed. At pH > 8.6 no reliable spectra could be obtained due to formation of a precipitate.

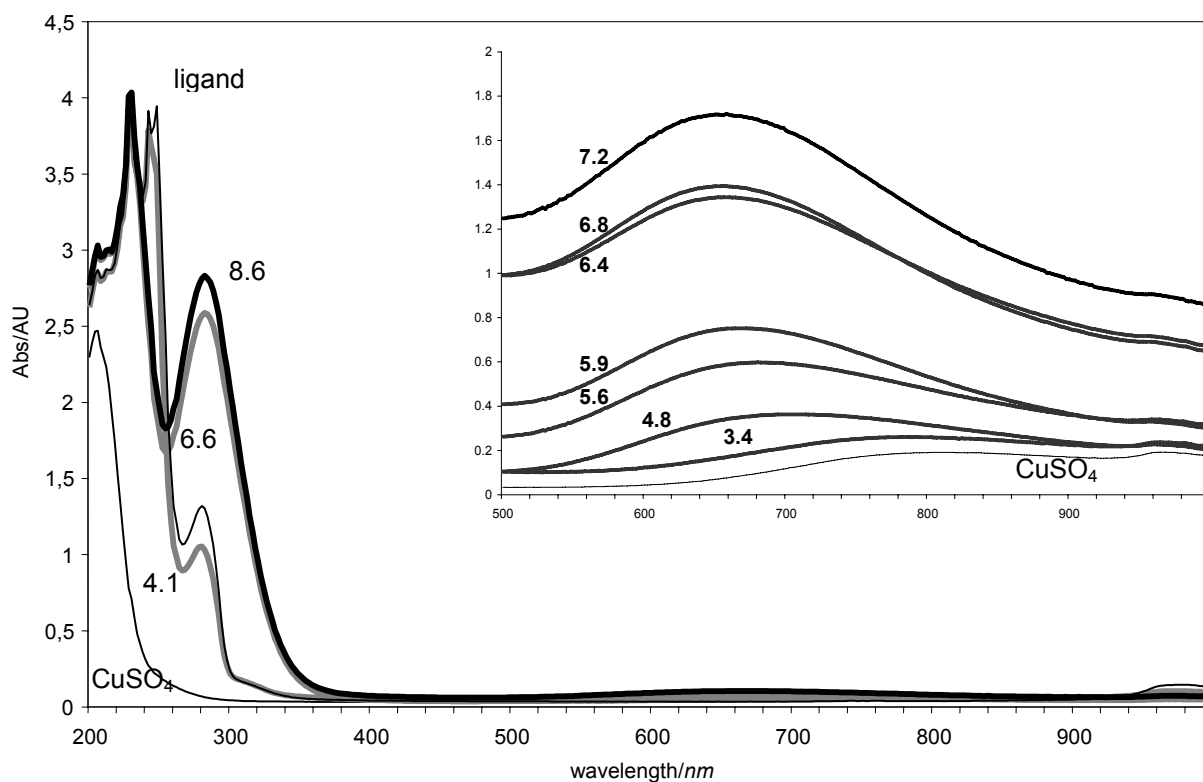


**Figure S6** – Absorption spectra of the complex at different pH (values are given at the curves in the graph). The main spectrum especially shows the charge transfer bands of a 5 mM solution (the Cu(II)-solution and ligand solution are shown by the narrow lines), the enlargement shows the *d-d* transition bands of a 25 mM solution. The change in intensity is clearly seen in the enlarged insert.

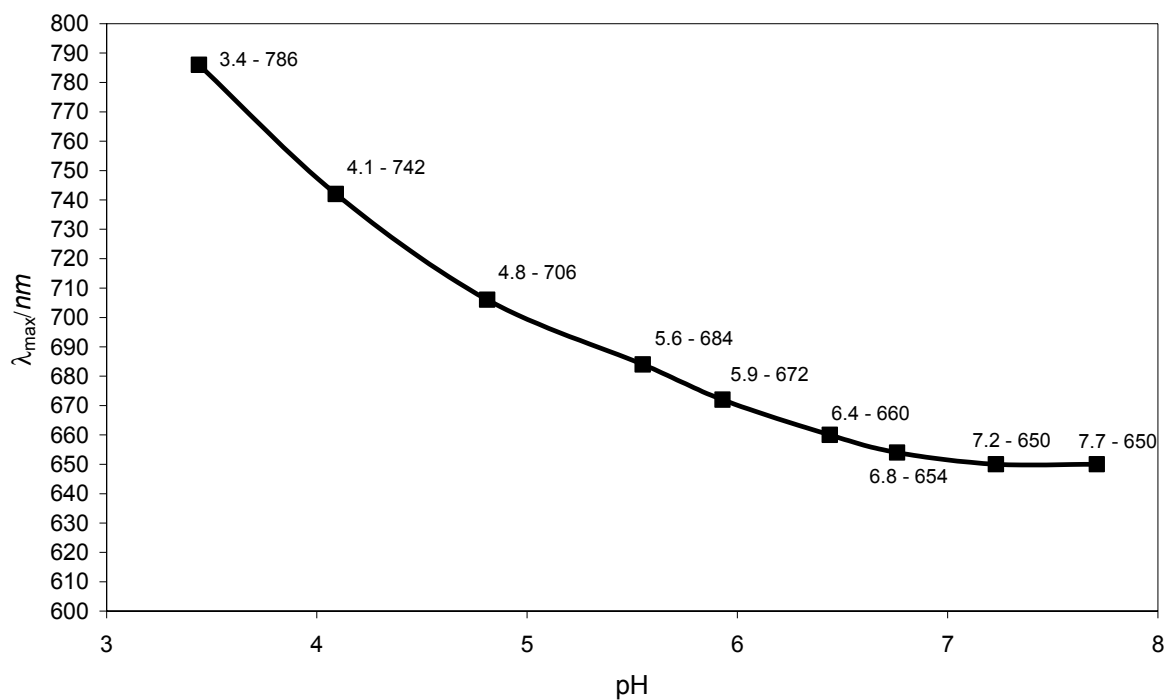
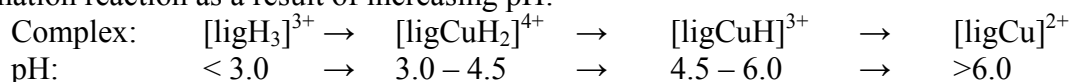


**Figure S7** – Shift in absorption maximum as a result of the change in pH.

The pH-titration (**figure S4**) curve already showed the following sequence concerning the coordination reaction as a result of increasing pH:



It can be inferred that at pH 4.1 the first imidazole ring of the tridentate ligand is coordinating to the cupric ion; the small shift in intensity (**figure S7**) shows no significant change in geometry at this stage. At pH 4.8, two coordinating imidazole rings are available and the measured absorption maximum corresponds to the presence of two N-ligands and two O-ligands in a square-planar geometry (measured: 706 nm, calculated<sup>6</sup>:  $684 \pm 11$  nm). The intensity of the absorption is still low, indicating a geometry with high centro-symmetry. With increasing pH, the third imidazole ring becomes available for coordination and from pH 5.9 to 6.4, a major increase in intensity is shown (**figure S6 and S7**). This indicates a major change in geometry in which the centro-symmetry is lost and the *d-d* transitions become Laporte allowed<sup>7</sup>. Even more, the square-planar geometry with three imidazole ligands should have an absorption band at  $629 \pm 13$  nm, which is 21 nm lower than the observed absorption. The most likely explanation for this is a change from square-planar with the two-coordinating imidazoles (and two water molecules), to a more tetrahedral like geometry with three imidazole rings and one water molecule. Alternatively, a distorted square-planar geometry can be envisioned (**figure S8**). Such a distortion from square-planar geometry should result in a smaller HOMO LUMO energy difference, thereby shifting the absorption maximum to slightly higher wavelengths.

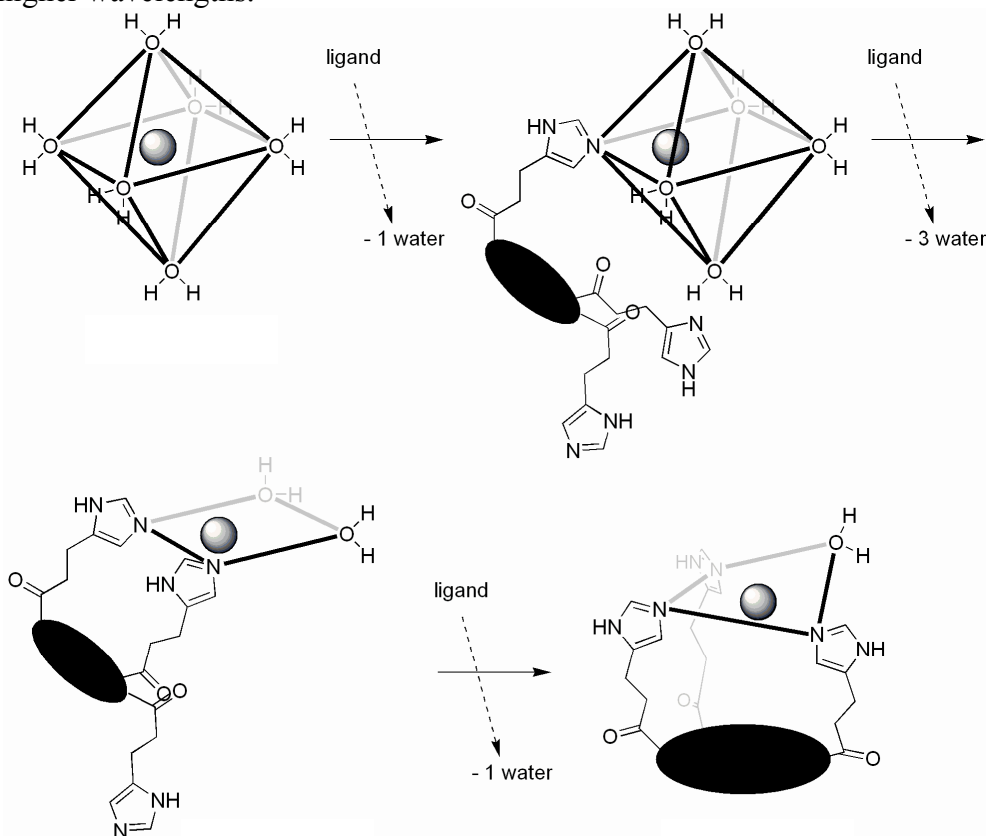


**Figure S8** – Suggested mechanism of coordination. The black sphere symbolizes the TAC-scaffold.

<sup>6</sup> E.J. Billo, *Inorg. Nucl. Chem. Lett.*, 1974, **10**, 613.

<sup>7</sup> B.N. Figgis and M.A. Hitchman, *Ligand Field Theory and Its Applications*, 1<sup>st</sup> edition, 2000, Wiley, USA.

## Infrared Spectra

Infrared spectra were obtained from freshly lyophilized samples (pH 7). These were mixed with KBr and pressed into a pellet that could be measured on the infrared spectrophotometer. Assignments were done using references for **table S1**.

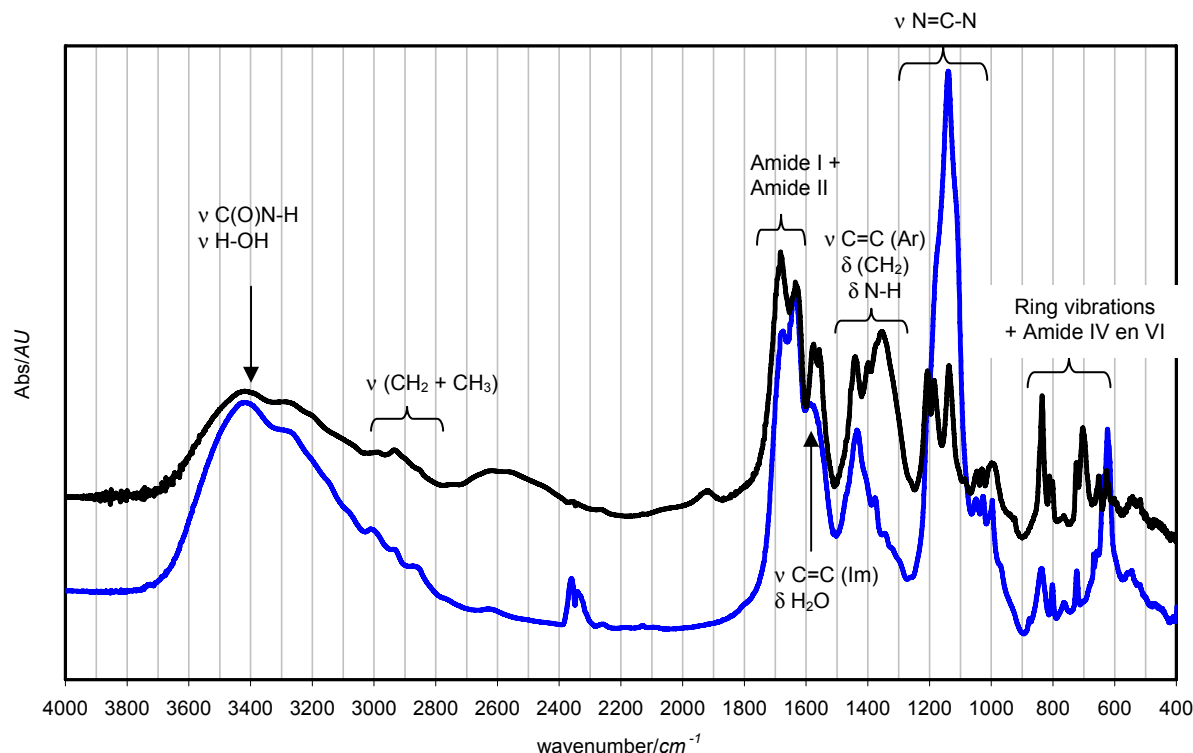


**Figure S9** – Full-width infrared spectrum of both ligand (black) and complex (blue).

As indicated in **figure S9**, the main functional groups present in the molecule are clearly visible. Around  $3400\text{ cm}^{-1}$  the amide C(O)N-H (both secondary and tertiary) stretching vibrations are situated, together with the coordinated water HO-H stretching vibrations (the presence of this water is more conclusively proven by an absorption at  $1595\text{ cm}^{-1}$ ). In the area of  $2800\text{--}3000\text{ cm}^{-1}$ , the symmetric and anti-symmetric stretching vibrations of the triazacyclophane-ring  $\text{CH}_2$  and the  $\text{C}^\beta\text{H}_2$  of the histidine amino acids, together with the acetyl- $\text{CH}_3$  are located. There is a broad absorption in the spectrum of the ligand around  $2600\text{ cm}^{-1}$ , which might indicate the presence of a protonated histidine residue (see also **figure S4**)<sup>8</sup>. This broad absorption is not present in the complex. The Amide-I and Amide-II vibrations are situated between  $1600$  and  $1700\text{ cm}^{-1}$ . Just below  $1600\text{ cm}^{-1}$ , vibrations that are important for the imidazole ring are found. Several bending vibrations are found between  $1300$  and  $1450\text{ cm}^{-1}$ , of which the most important ones are assigned to  $\text{CH}_2$  and N-H bending vibrations. The coordination of the imidazole ring to the copper(II) ion leads to a remarkable increase in intensity of the vibrations originating from the NCN-part of the imidazole ring ( $1100\text{--}1200\text{ cm}^{-1}$ ). An important absorption originating from the CC-N vibration is found at  $\sim 1000\text{ cm}^{-1}$ . The spectrum of the ligand reveals the presence of both tautomers, whereas the spectrum of the complex only shows the  $\text{N}^\pi$ -tautomer. Also, some changes are found in the low-wavenumber region of the spectrum ( $<900\text{ cm}^{-1}$ ), these originate from ring torsion and ring deformation vibrations (**figure S10**). Some of the above made comments have been evaluated in more detail in **table S1**.

<sup>8</sup> See for instance K.S. Broo, H. Nilsson, J. Nilsson, A. Flodberg, L. Baltzer, *J. Am. Chem. Soc.*, 1998, **120**, 4063.

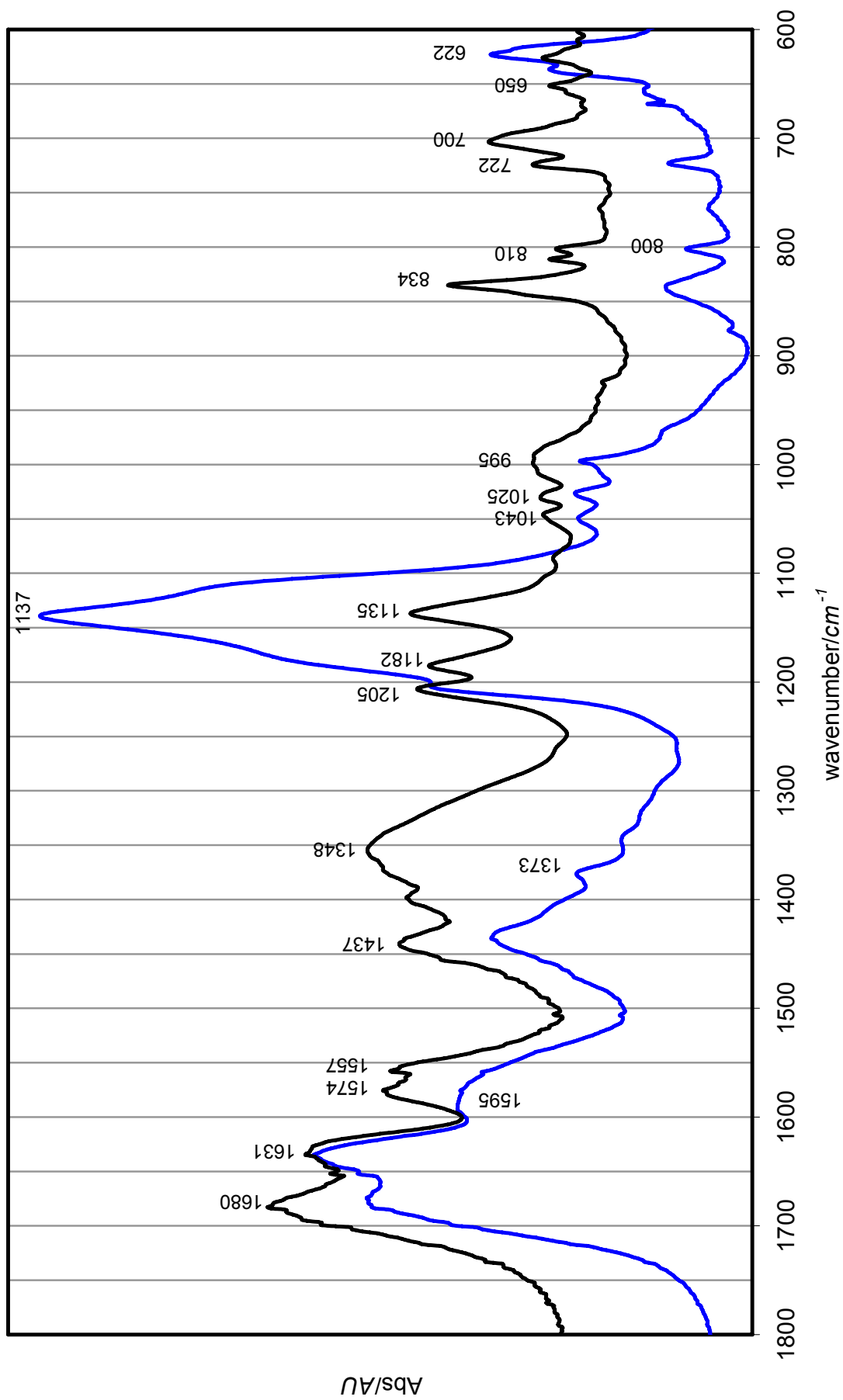
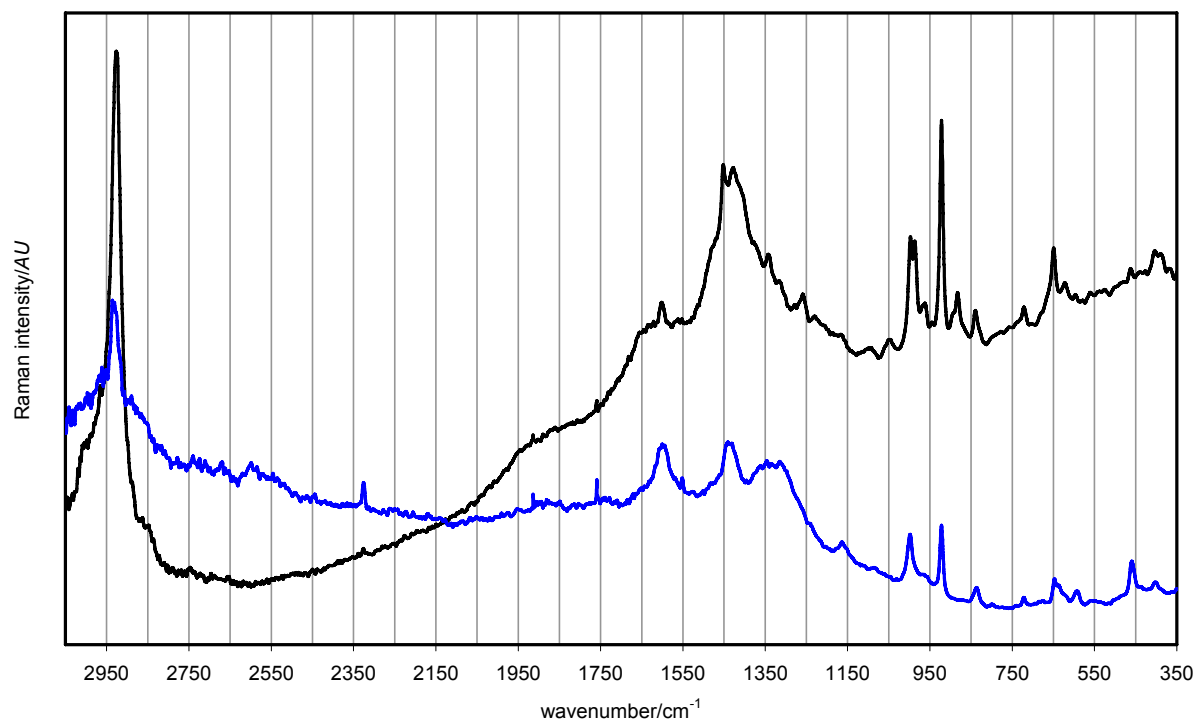


**Figure S10** – Infrared spectrum of ligand (black) and complex (blue).

## Raman Spectra

Raman spectra of both ligand and complex were obtained from freshly lyophilized samples (pH 7). Unfortunately, neither from concentrated solutions, nor from the lyophilized samples, any Raman intensities could be measured. The former had intense background fluorescence, whereas the latter was incinerated upon irradiation. By applying a drop of water to the powder a gel-like substance was formed in which the heat of the incoming radiation could be dispersed over present water molecules.

**Figure S11** – Full-width Raman spectrum of both ligand (black) and complex (blue).



The most intense peak is found at 2925 cm<sup>-1</sup> and this corresponds to aliphatic C-H stretching vibrations. At a wavenumber of about 1700 cm<sup>-1</sup>, a slight increase in intensity is found, corresponding to very weak Amide-I vibrations. Signals arising from CH-bending vibrations are found around 1450 and at 921 cm<sup>-1</sup>. More importantly however, are the vibrations at 458 and 588 cm<sup>-1</sup> and the vibrations at 1600 and 985-997 cm<sup>-1</sup> (**figure S12**). The former correspond to the Cu-N and Cu-O bond, respectively. The latter indicate the presence of both tautomeric forms (N<sup>π</sup> and N<sup>τ</sup>) of the histidinyI imidazole functionality in the ligand (doublet at 986 and 997 cm<sup>-1</sup>), but also show that the N<sup>π</sup>-tautomer is predominantly present in the complex (intense peak at 1600 and singlet at 997 cm<sup>-1</sup>). This means that coordination to the cupric ion is mostly via the N<sup>τ</sup>-atom of the imidazole ring of histidine. Additionally, this coordination to the metal ion leads to an increase in polarisability during vibration, what is in line with the increasing intensity of the ring stretch vibrations in the area of 1310-1350 cm<sup>-1</sup>.

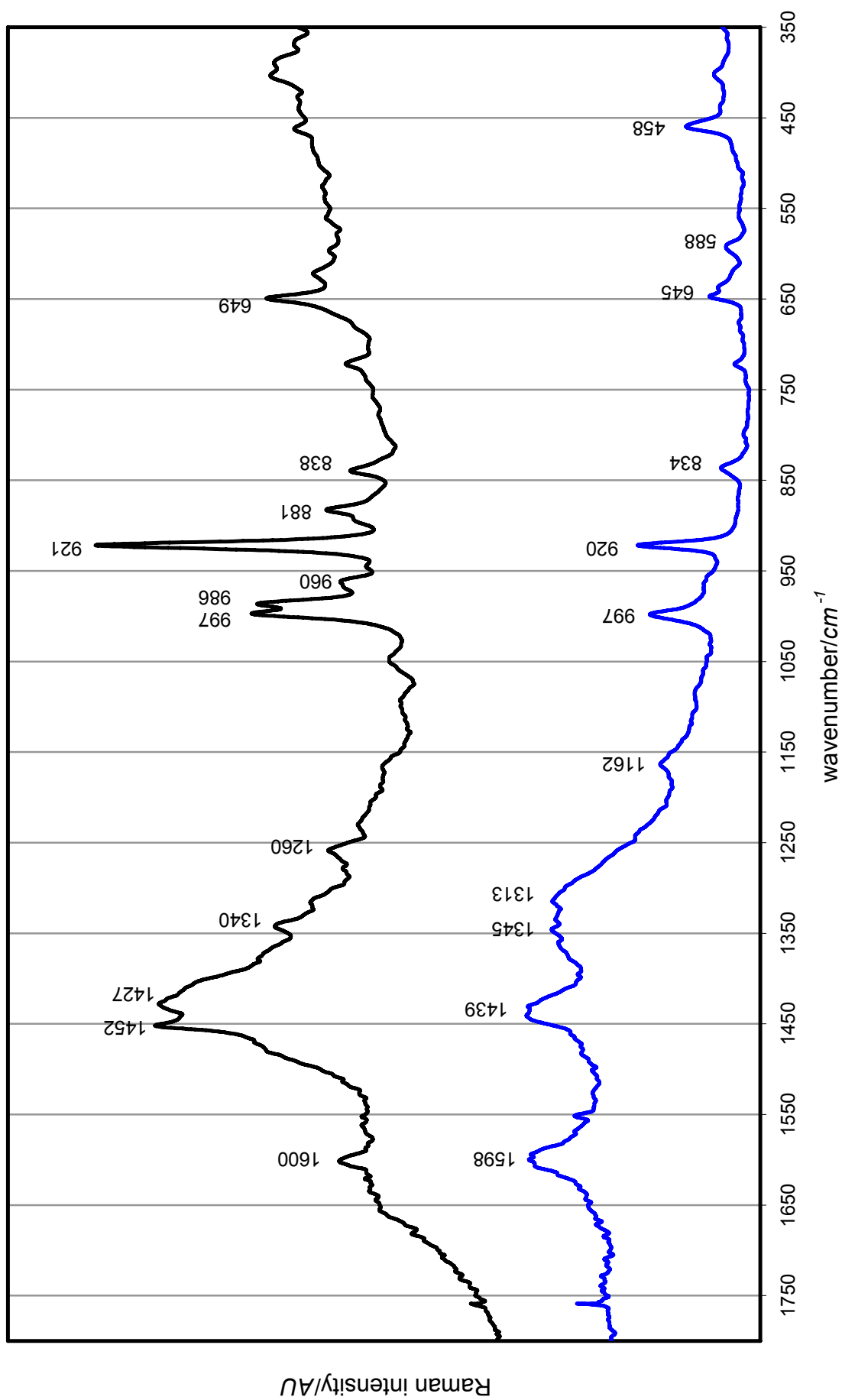


**Figure S12** – Raman spectrum ligand (black) and complex (blue).

**Table S1** – Proposed assignment for both IR and Raman signals.

IR		Raman		Assignment <sup>9</sup>
Ligand	Complex	Ligand	Complex	
3420-3200 (m, br)				$\nu$ C(O)N-H + $\nu$ H-OH
2983 (w)				$\nu_a$ CH <sub>3</sub>
2931 (w)	2931 (w)	2925 (vs)	2925 (vs)	$\nu_a$ CH <sub>2</sub>
2855 (w, sh)	2871 (w)			$\nu_s$ CH <sub>2</sub> + CH <sub>3</sub>
2619 (w, br)				$\nu$ Im <sup>+</sup> -H
1680 (s)	1674 (s)			Amide I
1651 (s)				Amide II
1631 (s)	1632 (s)			$\nu$ C=C*
		1600 (w)	1598 (s)	$\nu$ C=C* (N <sup>π</sup> ) / $\nu$ C=C (Ar)
	1595 (m)			$\nu$ C=C* (N <sup>π</sup> ) / $\delta$ H <sub>2</sub> O
1574 (m)	1573 (m, sh)			$\nu$ C=C* (N <sup>π</sup> )
1557 (m)	1559 (m, sh)		1550 (w)	$\delta$ N-H* / $\nu$ C(O)-N
		1452 (s)		$\nu$ ring* / $\omega$ CH <sub>2</sub>
1437 (m)	1435 (m)		1439 (s)	$\delta$ N-H* / $\nu$ C=C* / $\delta$ CH <sub>2</sub> / $\delta_a$ CH <sub>3</sub>
		1427 (s)	1429 (s)	$\delta$ N-H* / $\nu$ C=C* / $\delta$ CH <sub>2</sub>
1398 (m)				$\nu$ C(O)-N
1369 (m, sh)	1373 (w)			$\delta_s$ CH <sub>3</sub>
1348 (s)			1355 (m)	$\nu$ C(O)-N / $\nu$ ring*
	1342 (w)	1340 (w)	1345 (m)	$\nu$ C(O)-N / $\nu$ ring*
	1320 (w, sh)		1329 (m), 1313 (m)	$\nu$ C(O)-N / $\nu$ ring*
	1300 (w, sh)			$\nu$ C=N + $\delta$ =C-H
		1273 (w)	1267 (w, sh)	$\nu$ ring* (N <sup>π</sup> ) / $\delta$ CH <sub>2</sub> / Amide III
		1260 (w)		$\nu$ ring* (N <sup>π</sup> ) / Amide III
			1239 (w)	$\nu$ ring* (N <sup>π</sup> ) / $\tau$ CH <sub>2</sub>
1205 (m)	1199 (m)			$\nu$ NCN
1182 (m)	1166 (s, sh)		1162 (w)	$\nu$ NCN + $\delta$ N-H*
1135 (m)	1137 (vs)			$\nu$ =C-N= + $\delta$ N-H*
1084 (w)				$\nu$ C(O)-N
1043 (w)	1048 (w)			$\delta$ C-H* / $\delta$ C <sup>Ar</sup> -H (ip)
1025 (w)	1026 (w)			$\delta$ C <sup>Ar</sup> -H (ip)
995 (br)	997 (w)	997 (m)	997 (s)	$\delta$ C-N* (N <sup>π</sup> )
		986 (m)		$\delta$ C-N* (N <sup>π</sup> )
		960 (w)	960 (w)	$\nu$ =C-N + $\delta$ ring
		921 (s)	920 (s)	$\delta$ C-H (ip) (NCN)
	875 (vw)	881 (w)		$\delta$ ring
834 (m)	834 (w)	838 (w)	834 (w)	$\delta$ ring
800 (w)	800 (w)			$\delta$ C <sup>Ar</sup> -H (oop)
763 (vw)	764 (vw)			$\delta$ C-H* (oop)
722 (w)	723 (w)		719 (w)	$\delta$ N-H (oop) / $\rho$ CH <sub>2</sub> (ip) / $\delta$ C <sup>Ar</sup> -H (oop)
700 (m)	668 (w)			Ring torsion*
650 (w)	655 (w)	649 (m)	645 (m)	Ring torsion*
	636 (w)		636 (w)	Ring torsion*
625 (w)	622 (m)			Ring torsion*
			588 (w)	$\nu$ Cu-O
			458 (m)	$\nu$ Cu-N

**Used abbreviations** In the peak section: s = strong, m = medium, w = weak, v = very, sh = shoulder, br = broad. In the assignment section:  $\nu$  = stretching,  $\delta$  = bending,  $\rho$  = rocking,  $\tau$  = twisting,  $\omega$  = wagging, subscript s = symmetric, subscript a = asymmetric, \* = imidazole ring vibrations, N<sup>π</sup> = tautomer in which N<sup>π</sup> is protonated, N<sup>τ</sup> = tautomer in which N<sup>τ</sup> is protonated, ip = in plane, oop = out of plane, C<sup>Ar</sup> = aromatic ring (from the scaffold), + = coupled vibrations, / = isolated vibrations.

<sup>9</sup> R.M. Silverstein and F.X. Webster, *Spectrometric Identification of Organic Compounds*, 6<sup>th</sup> edition, 1998, Wiley, USA; K. Nakamoto, *Infrared and Raman Spectra of Inorganic and Coordination Compounds* – part A and especially part B, 5<sup>th</sup> edition, 1997, Wiley, USA; J.G. Mesu, T. Visser, F. Soulimani, B.M. Weckhuysen, *Vibr. Spectrosc.*, 2005, **39**, 114; J.B. Hodgson, G.C. Percy, D.A. Thornton, *J. Mol. Struct.*, 1980, **66**, 81; J.G. Mesu, T. Visser, F. Soulimani, E.E. van Faassen, P. de Peinder, A.M. Baelle, B.M. Weckhuysen, *Inorg. Chem.*, 2006, **45**, 1960; A. Torreggiani, M. Tamba, G. Fini, *Biopolymers*, 2000, **57**, 149; A. Torreggiani, M. Tamba, S. Bonora, G. Fini, *Biopolymers*, 2003, **72**, 290; T. Miura, T. Satoh, A. Hori-i, H. Takeuchi, *J. Raman Spectr.*, 1998, **29**, 41; T. Miura, A. Hori-i, H. Mototani, H. Takeuchi, *Biochemistry*, 1999, **38**, 11560.

### Oxygen binding and activation by the Cu(I)-complex

The oxygen-binding ability of the Cu(I)-complex was assessed by UV/vis spectroscopic analysis of the Cu(I)-complex in solution (DMSO). Condensed product was analyzed by diffuse reflection, infrared and Raman spectroscopy.

**Reaction conditions.** To a solution of the ligand (40 mM; 200  $\mu$ L) in DMSO was added a freshly prepared solution of  $[\text{Cu}(\text{MeCN})_4](\text{PF}_6)$  (29.2 mM; 274  $\mu$ L) in DMSO. This resulted in a 17 mM solution of the complex which was suitable for analysis of the *d-d* transitions. This clear solution was analyzed immediately after preparation. Nevertheless, the initial change in colour from colourless to pale blue could not be monitored by absorption spectroscopy. The time between the obtained spectra and the preparation of the complex was approximately two minutes. For the analysis of the charge-transfer bands a 2.5 mM solution was used.

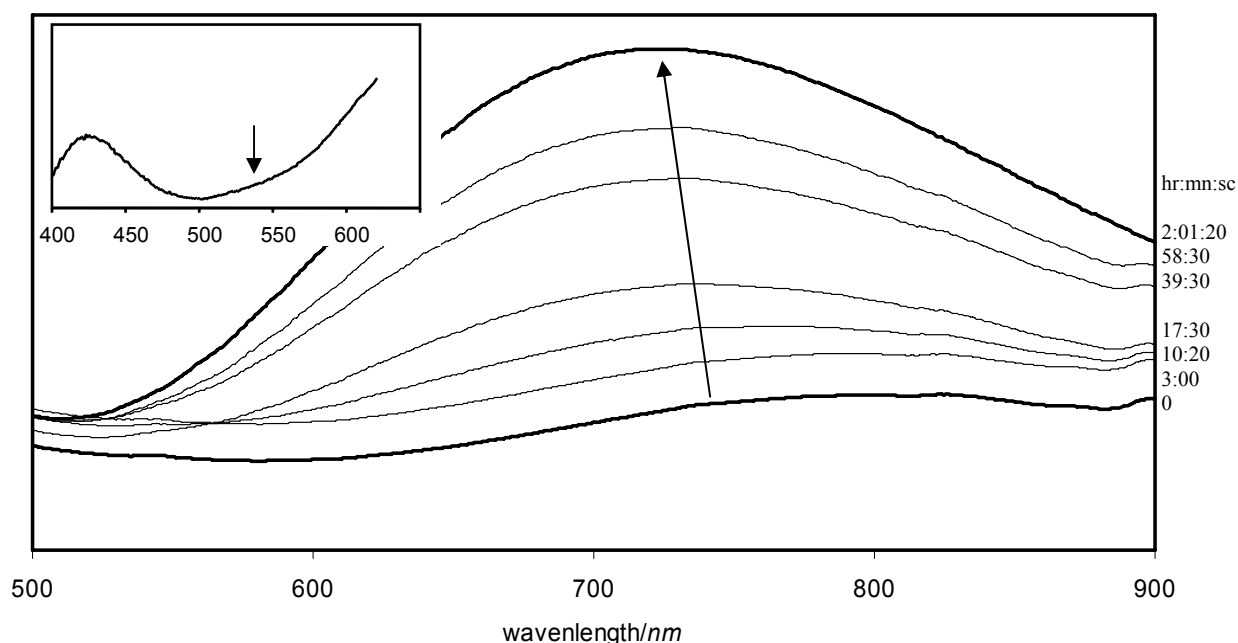


**Figure S13** – UV/vis absorption spectrum of the *d-d* transition bands of the Cu(I)-complex as a function of time. The arrow indicates the increment and blue-shift of a shoulder of the absorption maximum of the first measurement. Insert: diffuse reflection spectrum of condensed complex (arrow indicates the absorption plateau around 540 nm).

The main feature of this spectrum is the shift of the absorption maximum from 825 nm to 722 nm (**figure S14**). The fact that the solution obtains a blue-green colour indicates that copper(II) is formed<sup>10</sup>. Two other absorptions are found by diffuse reflection spectroscopy: a clear band at 423 nm and a plateau at 540 nm. The absorption maximum of 722 nm corresponds nicely with a square-pyramidal geometry at the copper(II)-centre in which the four equatorial positions are occupied by two nitrogen (from the ligand) and two oxygen atoms (from the oxygen molecule) and the axial position is occupied by the nitrogen atom of the remaining imidazole ring of the tridentate ligand.

<sup>10</sup> S. Mahapatra, J.A. Halfen, E.C. Wilkinson, G. Pan, C.J. Cramer, L. Que, Jr and W.B. Tolman, *J. Am. Chem. Soc.*, 1995, **117**, 8865.

Based on calculations, this square-pyramidal geometry should have an absorption maximum of  $734 \pm 10 \text{ nm}^{11}$ . From **figure S14** can be seen that after 15 minutes this geometry is formed which then equilibrates during 90 minutes towards a complex with an absorption maximum at 722 nm.

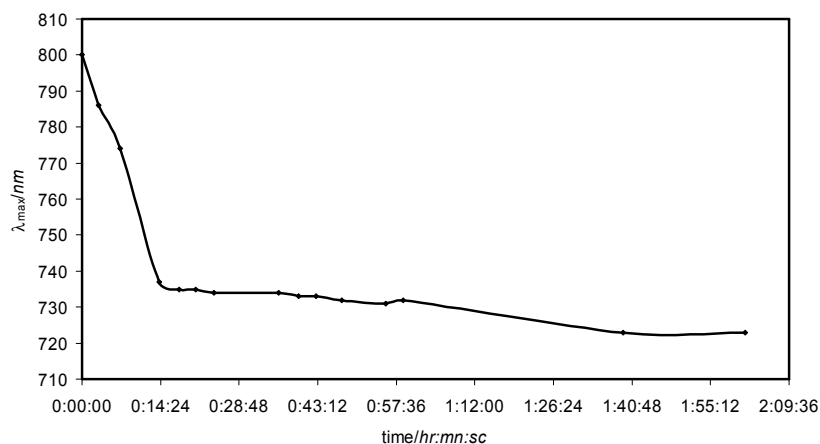


**Figure S14** – Shift of the absorption maximum as a result of the oxygen uptake, monitored in time (min).

Since this complex is prepared in DMSO (a very hygroscopic solvent) at room temperature, we anticipated that the formed complex is the bis( $\mu$ -hydroxo) dicopper(II) complex (**figure S15**). It is known that the ( $\mu$ - $\eta^2$ : $\eta^2$ )-peroxo dicopper(II) complex is stable at low temperature (usually around  $-80 \text{ }^\circ\text{C}$ ), and that it easily decomposes into the bis( $\mu$ -oxo) dicopper(III) complex<sup>12</sup>. Further decomposition – as result of higher temperature, moisture or even ligand cleavage – usually leads to the bis( $\mu$ -hydroxo) dicopper(II) species<sup>13</sup>. More evidence on the type of CuO-species could be obtained from IR and Raman spectroscopy, although the UV/vis-spectrum (**figure 3** and **S13**) already showed that it could not be the ( $\mu$ - $\eta^2$ : $\eta^2$ )-peroxo complex (absorptions at 350 and 550 nm) nor the bis( $\mu$ -oxo) complex (absorptions at 300 and 400 nm).

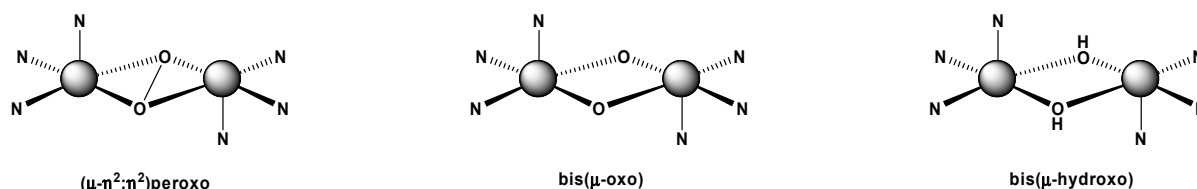


**Figure S15** – Different CuO-complexes based on the N,N,N,O,O-square-pyramidal coordination round copper.

<sup>11</sup> E.J. Billo, *Inorg. Nucl. Chem. Lett.*, 1974, **10**, 613. See also: Z.D. Matović, G. Pelosi, S. Ianelli, G. Ponticelli, D.D. Radanovic and D.J. Radanovic, *Inorg. Chimica Acta*, 1998, **268**, 221; U. Rychlewska, Z.D. Matović, D.D. Radanovic, M.Dj. Dimitrijevic, D.M. Ristanovic, M.M. Vasojevic and D.J. Radanovic, *Polyhedron*, 2001, **20**, 2523; K. Itoh, H. Hayashi, H. Furutachi, T. Matsumoto, S. Nagatomo, T. Tosha, S. Terada, S. Fujinami, M. Suzuki and T. Kitagawa, *J. Am. Chem. Soc.*, 2005, **127**, 5212.

<sup>12</sup> J.A. Halfen, S. Mahapatra, E.C. Wilkinson, S. Kaderli, V.G. Young Jr, L. Que Jr, A.D. Zuberbühler and W.B. Tolman, *Science*, 1996, **271**, 1397; C.J. Cramer, B.A. Smith and W.B. Tolman, *J. Am. Chem. Soc.*, 1996, **118**, 11283; A. Bérces, *Inorg. Chem.*, 1997, **36**, 4831; P.L. Holland, W.B. Tolman, *Coordination Chemistry Reviews*, 1999, **190-192**, 855.

<sup>13</sup> J. Gao and S.-h. Zhong, *J. Mol. Catal. A: Chem.*, 1999, **164**, 1; L. Que, Jr. and W.B. Tolman, *Angew. Chem. Int. Ed.*, 2002, **41**, 1114; L. Q. Hatcher and K.D. Karlin, *J. Biol. Inorg. Chem.*, 2004, **9**, 669; W.B. Tolman, *Acc. Chem. Res.*, 1997, **30(6)**, 227; E.A. Lewis and W.B. Tolman, *Chem. Rev.*, 2004, **104**, 1047-1076.

## Infrared and Raman analysis of the CuO-complex

The spectra were obtained using a dried sample of the CuO-complex. Additional literature for the assignment can be found in the references of **table S1**.

### Infrared (KBr)

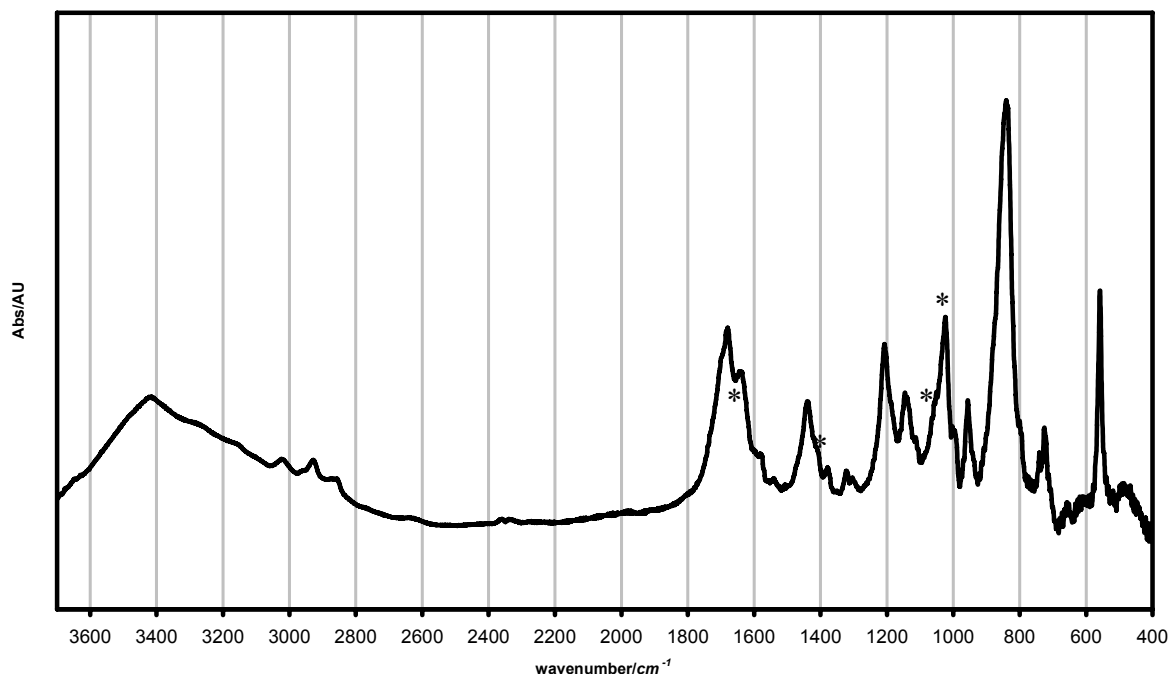


**Figure S16** – IR spectrum of the dried CuO-complex (\* = DMSO).

This spectrum shows a relatively sharp broad peak at  $3400\text{ cm}^{-1}$ , this peak is sharper than the corresponding peak in the spectrum of the Cu(II)-complex (**figure S9**). This peak corresponds to the O-H stretching vibrations of the hydroxyl-bridges between the two copper ions in the  $\text{Cu}_2(\text{OH})_2$ -species supposed to be present in our complex<sup>14</sup>. Although such a bridging H-O stretching vibration is usually found at higher wavenumbers ( $3650\text{ cm}^{-1}$ ) as a sharp peak, it is known that hydrogen bonding shifts it to lower wavenumbers and broadens the peak<sup>15</sup>. Also remarkable is the change in intensity of the intense absorption at  $1137\text{ cm}^{-1}$  found in the Cu(II)-complex: this has disappeared and two medium intense peaks emerged on similar positions as the triple-peaks in the spectrum of the ligand. The peak at  $817\text{ cm}^{-1}$  corresponds to vibrations of the  $\text{PF}_6^-$ -anion. Just below  $1600\text{ cm}^{-1}$  ( $1584\text{ cm}^{-1}$ ) and around  $1000\text{ cm}^{-1}$  ( $1003$  and  $999\text{ cm}^{-1}$ ) small signals originating from the  $\text{N}^{\tau}$ -tautomeric C=C stretching and  $\text{C}^2$ -H bending vibrations are found (**figure S17**). These signals are much more pronounced in the Raman spectrum, but are observed here too. Concerning the kind of CuO-species, the peak at  $957\text{ cm}^{-1}$  corresponds to di-copper bridging hydroxyl groups<sup>15</sup>. A sample prepared in  $\text{DMSO-d}_6$  with a small amount of  $\text{D}_2\text{O}$  shows that this peak has disappeared and a peak emerged at  $761\text{ cm}^{-1}$ , indicating the change of hydroxo- to deuteroxo-bridges<sup>16</sup>. More evidence on the  $\text{Cu}_2\text{O}_2$ -core could be found in the Raman spectrum. For the remaining signals the interpretation as made for the Cu(II)-complex applies (see also **table S2**).

<sup>14</sup> S. Mahapatra, J.A. Halfsen, E.C. Wilkinson, G. Pan, X. Wang, V.G. Young Jr., C.J. Cramer, L. Que Jr. and W.B. Tolman, *J. Am. Chem. Soc.*, 1996, **118**, 11555.

<sup>15</sup> J.R. Ferraro and W.R. Walker *Inorg. Chem.*, 1965, **10(4)**, 1382.

<sup>16</sup> See for instance the book of Nakamoto in ref 9 in the Supplementary Information.

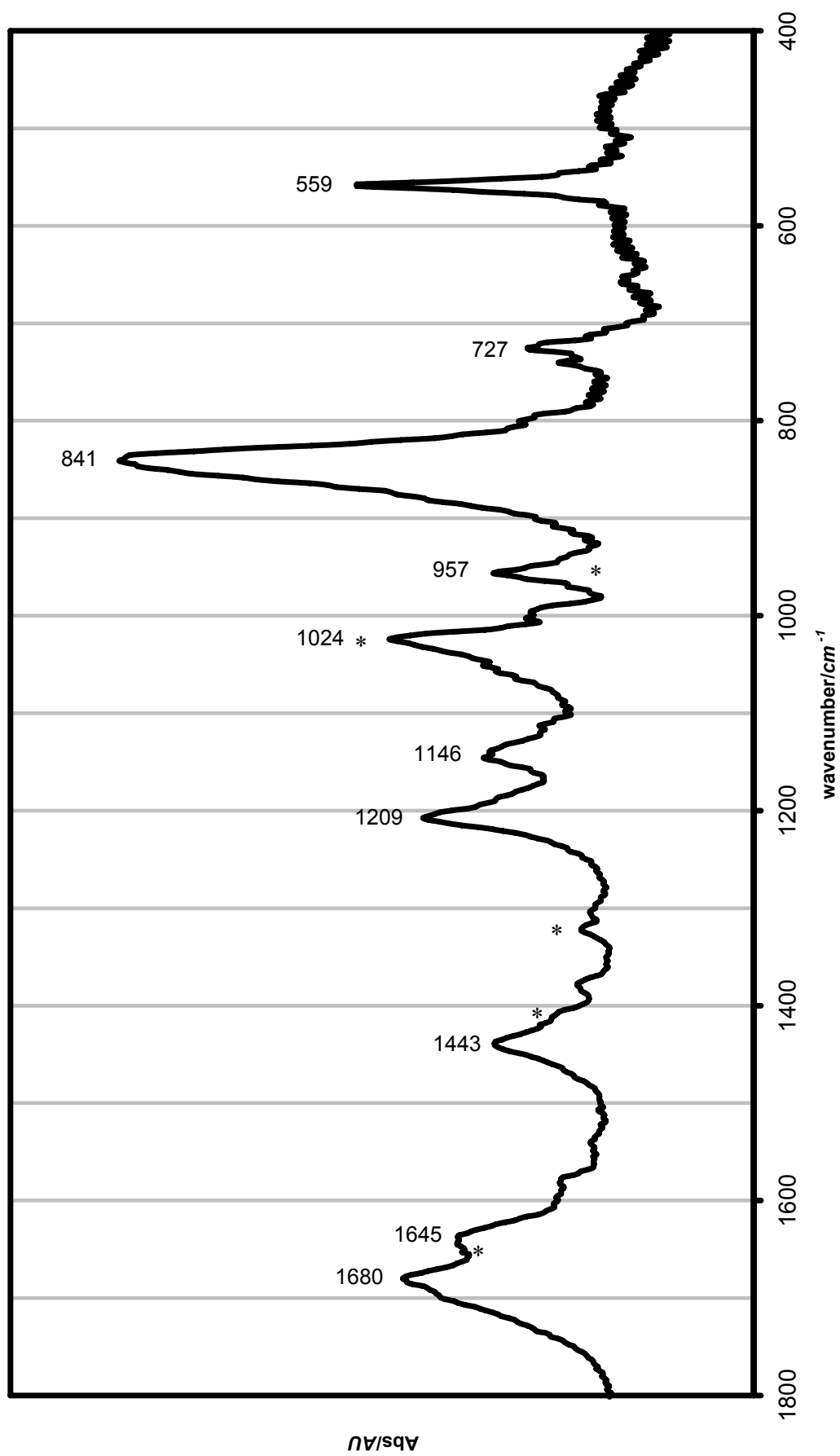


**Figure S17** – Infrared spectrum of the CuO-complex (\* = DMSO).

## Raman

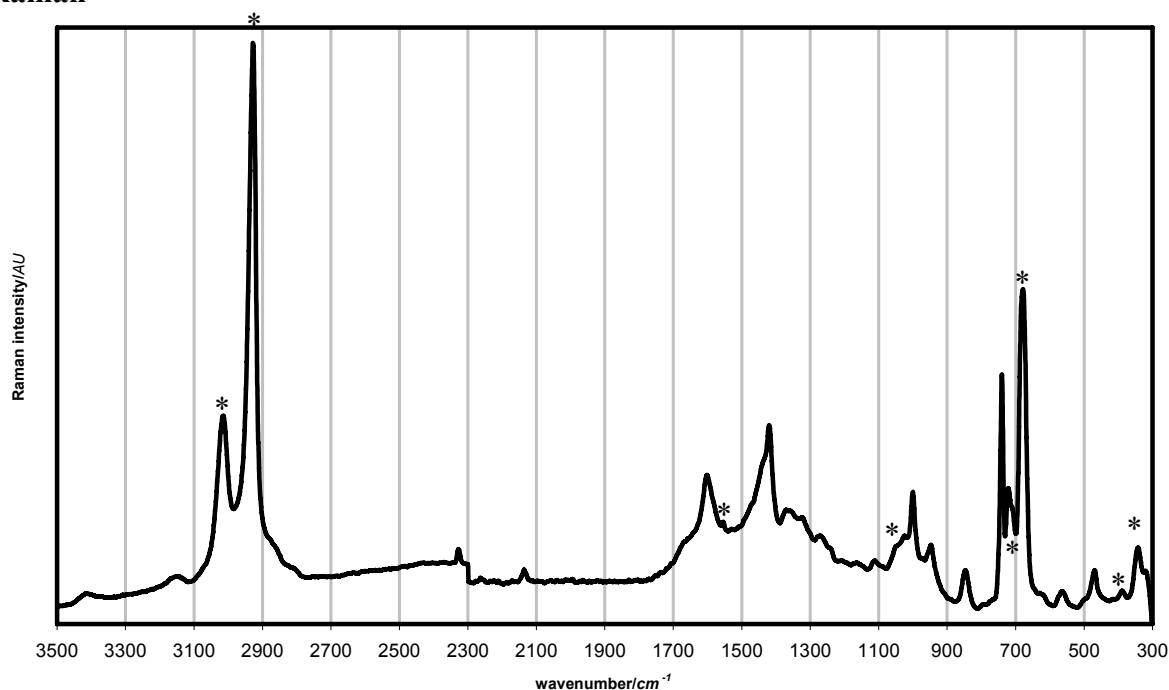


**Figure S18** – Raman spectrum of the CuO-complex (\* = DMSO).

Comparison of this spectrum with the spectrum of the Cu(II)-complex (**figure S11 and S12**) yields valuable information on the tautomeric forms of the binding imidazole ligands and also additional information on the properties of the CuO-complex. For instance, since this complex is obtained from a solution of DMSO, signals from this solvent can still be observed in the spectrum, they are marked with an asterisk. Concerning the binding tautomeric form of the imidazole ring, the peaks at 1600 and 1000  $\text{cm}^{-1}$  unambiguously show that the  $\text{N}^{\pi}$ -tautomer is predominantly present and that the  $\text{N}^{\tau}$ -nitrogen atom is coordinated to the copper centre. Also, the Cu-O and Cu-N bonds are seen in this spectrum, although at slightly different wavenumbers than in the Cu(II)-complex (**figure S19**). The Cu-O intensity shifts from 588 to 568  $\text{cm}^{-1}$ , which can be explained by the bridging nature of the hydroxyl group: although the charge on the oxygen atom increases (when compared to water, **figure S12**), it is now bound to two copper-ions, making each individual Cu-O bond less strong<sup>17</sup>. Concerning the Cu-N bond, this is now shifted to 472  $\text{cm}^{-1}$  whereas in the Cu(II)-complex this was found at 458  $\text{cm}^{-1}$ . These shifts identify an increase in energy of the Cu-N bonds. In the square-planar geometry change from N,N,N,O- to N,N,O,O-coordination, the replacement of a strong coordinating nitrogen atom with a weaker coordinating oxygen atom could allow a stronger coordination of the two remaining nitrogen atoms. A weak peak at 392  $\text{cm}^{-1}$  might correspond to the weaker axial coordinating nitrogen atom of the imidazole ring, although overlap with a DMSO peak at this wavelength might obscure this signal. With respect to the type of CuO-species present in the complex, the intense signal at 740  $\text{cm}^{-1}$  corresponds most likely to a symmetrical  $\text{Cu}_2\text{O}_2$ -diamond core breathing vibration<sup>18</sup>. Although most information of this  $\text{Cu}_2\text{O}_2$ -diamond core has been found by measuring  $(\mu\text{-}\eta^2\text{:}\eta^2)$ -peroxo and bis( $\mu$ -oxo) complexes, the intensity of the peak and the position being close to most vibrations of this

<sup>17</sup> W.R. McWhinnie, *J. Inorg. Nucl. Chem.*, 1965, **27**, 1063.

<sup>18</sup> J.A. Larrabee and T.G. Spiro, *J. Am. Chem. Soc.*, 1980, **102**(12), 4217; M.J. Henson, M. A. Vance, C. Xin Zhang, H.-C. Liang, K.D. Karlin and E.I. Solomon, *J. Am. Chem. Soc.*, 2003, **125**, 5186; A.P. Cole, V. Mahadevan, L.M. Mirica, X. Ottenwaelder and T.D.P. Stack, *Inorg. Chem.*, 2005, **44**, 7345.

type of  $\text{Cu}_2\text{O}_2$ -core, leads to the assignment of this signal to the  $\text{Cu}_2\text{O}_2$ -core symmetric stretching vibration. Even more, the decreased compactness of the diamond core<sup>19</sup> – when the bis( $\mu$ -hydroxo) and bis( $\mu$ -oxo) complexes are compared – should result in lowering the energy of the  $\text{Cu}_2\text{O}_2$ -core vibration. These  $\text{Cu}_2\text{O}_2$ -core vibrations are usually very strong in Raman and are even more enhanced when symmetrical compounds or complexes are considered. Another observation related to this supposed dimerisation that should be mentioned is the disappearance of the imidazole  $\text{C}^2\text{-H}$  in-plane bending vibration, found at 921 or 920  $\text{cm}^{-1}$  in the free ligand and Cu(II)-complex (**figure S11** and **S12**). This disappearance indicates major differences in the surroundings of these C2-H hydrogen atoms, probably originating from differences in geometry between the Cu(II)- and  $\text{Cu(II)}_2(\text{OH})_2$ -complexes. Apparently, the dimeric character of the CuO-species prohibits this bending motion.

---

<sup>19</sup> W.B. Tolman, *Acc. Chem. Res.*, 1997, **30(6)**, 227.

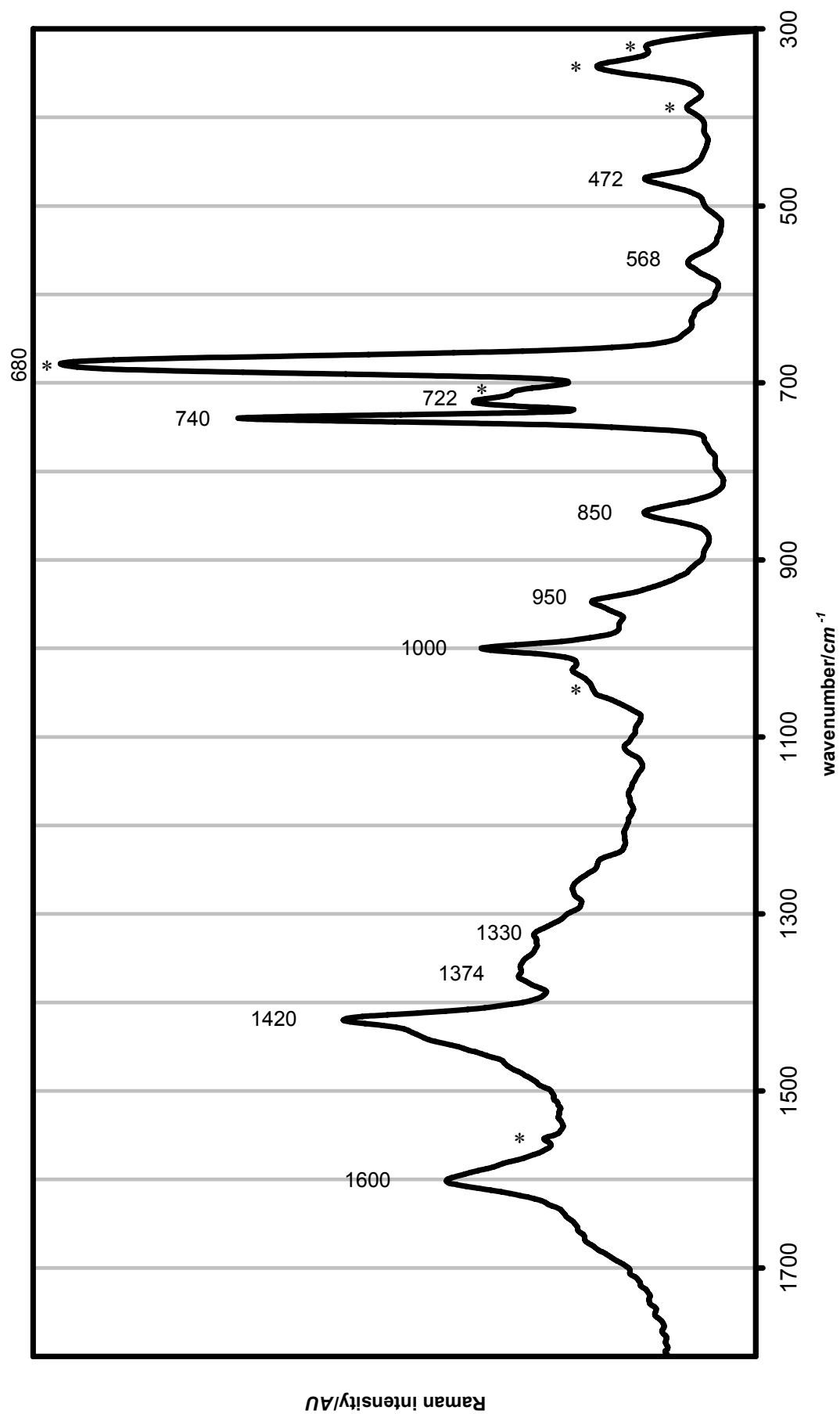


**Figure S19** – Raman spectrum of the CuO-complex (\* = DMSO).

**Table S2** – Proposed assignment for both infrared and Raman signals of the CuO-complex.

Infrared Complex	Raman Complex	Assignment <sup>9</sup>
3400 (br, m)		$\nu$ C(O)N-H / $\nu$ O-H (H-bonded)
2931 (w)	2925 (vs)	$\nu_a$ CH <sub>2</sub>
2871 (w)		$\nu_s$ CH <sub>2</sub> + CH <sub>3</sub>
1680 (m)		Amide I
1645 (m)		Amide II
	1600 (m)	$\nu$ C=C* (N <sup>π</sup> ) / $\nu$ C=C (Ar)
1584 (w)		$\nu$ C=C* (N <sup>π</sup> )
1443 (m)		$\delta$ N-H* / $\nu$ C=C* / $\delta$ CH <sub>2</sub> / $\delta_a$ CH <sub>3</sub>
	1420 (s)	$\delta$ N-H* / $\nu$ C=C* / $\delta$ CH <sub>2</sub>
		$\nu$ C(O)-N
1383 (w)	1374 (w)	$\delta_s$ CH <sub>3</sub>
	1330 (w)	$\nu$ C(O)-N / $\nu$ ring*
1209 (m)		$\nu$ NCN
1146 (m)		$\nu$ =C-N= + $\delta$ N-H*
1051 (w)		$\delta$ C-H* / $\delta$ C <sup>Ar</sup> -H (ip)
1024 (m)		$\delta$ C <sup>Ar</sup> -H (ip)
1003+999 (w)	1000 (m)	$\delta$ C-N* (N <sup>π</sup> )
957 (m)	950 (w)	$\nu$ =C-N + $\delta$ ring / $\delta$ CuO-H
	850 (w)	$\delta$ ring
841 (s)		PF <sub>6</sub> -ion
	740 (s)	Cu <sub>2</sub> OH <sub>2</sub> diamond core breathing
727 (w)	722 (m)	$\delta$ N-H (oop) / $\rho$ CH <sub>2</sub> (ip) / $\delta$ C <sup>Ar</sup> -H (oop)
	568 (w)	$\nu$ Cu-O
559 (s)		Ring torsion*
	472 (w)	$\nu$ Cu-N <sup>eq</sup>
	392 (m)	$\nu$ Cu-N <sup>ax</sup>

**Used abbreviations** In the peak section: s = strong, m = medium, w = weak, v = very, br = broad. In the assignment section:  $\nu$  = stretching,  $\delta$  = bending,  $\rho$  = rocking, subscript s = symmetric, subscript a = asymmetric, \* = imidazole ring vibrations, N<sup>π</sup> = tautomer in which N<sup>π</sup> is protonated, ip = in plane, oop = out of plane, C<sup>Ar</sup> = aromatic ring (from the scaffold), N<sup>ax</sup> = axial coordinating nitrogen atom, N<sup>eq</sup> = equatorial coordinating atom, + = coupled vibrations, / = isolated vibrations.

### Oxidative activity of the CuO-complex

In order to show the reversibility of the formed L<sub>2</sub>Cu<sub>2</sub>O<sub>2</sub>-complex, one equivalent (10  $\mu$ L of a 50 mM solution) of 3,5-di-*tert*-butylcatechol was added to the equilibrated complex (200  $\mu$ L, 2.5 mM) and the change in absorption spectrum was measured. This procedure was also carried out using an aged complex – three weeks on the bench – with identical results. Upon addition of the substrate, the colour of the complex immediately changed from mint-green to yellow.

## Modeling

For the construction of some computer models of the complexes, the YASARA computer modeling program<sup>20</sup> (version 6.8.13) was used. The ligand system was drawn using ChemDraw 9.0 and converted to the pdb-format with Chem3D 9.0. In YASARA copper(II) was added and, based on our findings in the presented spectrophotometric studies, the N<sup>T</sup>-nitrogen atoms of the imidazole rings were set to coordinate to the copper(II) ion. The force constant for fixating the position of the nitrogen atoms was 20 N/m and the distance was set at 2.0 Å (which is the average of the N-Cu distance in the protein active site). The force cut-off was set at 5.24 Å, in accordance with the suggested value and the Nova F force field was used. The minimized structure was overlaid with one side of the type-3 copper binding site of hemocyanin using DS Viewer Pro (**figure S19**).

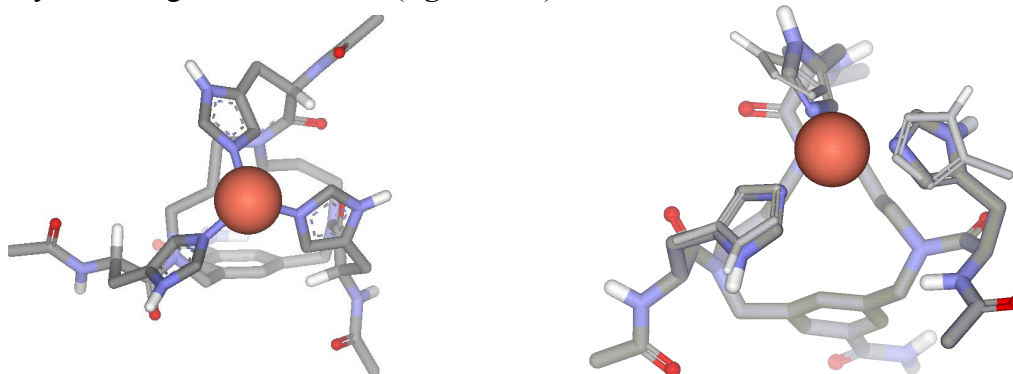


**Figure S19** – *Left*: minimized structure of the Cu(II)-complex; *right*: overlay of the minimized structure with one side of the type-3 copper binding site of hemocyanin.

As can be seen from these pictures, the synthesized tridentate ligand system is capable of mimicking the structure of one side of the type-3 copper binding site of hemocyanin; this includes the angle of approach of the histidinyll imidazole rings. To show the similarity between type-3 copper sites in different proteins, three different forms of type-3 copper active sites are shown below (**figure S20**). These were generated with DS Viewer Pro using the corresponding pdb-files.

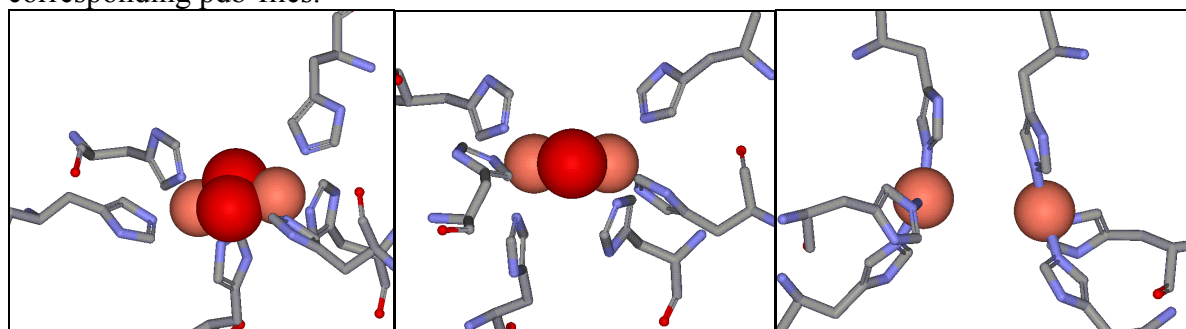


**Figure S20** – Active sites containing the 3-histidine facial triad binding to copper-ions. *Left*: tyrosinase<sup>21</sup> (1WX2, oxy-form), also found in oxygenated hemocyanin (code 1OXY); *middle*: catechol oxidase<sup>22</sup> (1BT3, met-form), this form is also found as the met-form in tyrosinase (code 1WX3); *right*: deoxygenated hemocyanin<sup>23</sup> (1LLA). Copper: pink spheres; oxygen: red spheres.

<sup>20</sup> [www.yasara.org](http://www.yasara.org). A NOVA server is freely accessible at <http://www.yasara.com/servers>. See also E. Krieger, G. Koraimann and G. Vriend, *Proteins*, 2002, **47**, 393.

<sup>21</sup> H. Decker, T. Schweikardt, F. Tucek, *Angew. Chem., Int. Ed.*, 2006, **45**, 4546.

<sup>22</sup> C. Gerdemann, C. Eicken, B. Krebs, *Acc. Chem. Res.*, 2002, **35**, 183.

<sup>23</sup> K.A. Magnus, B. Hazes, H. Ton-That, C. Bonaventura, J. Bonaventura, W.G.J. Hol, *Proteins: Structure, Function, and Genetics*, 1994, **19**, 302.